Symmetric Shape Morphing for 3D Face and Head Modelling

Hang Dai[1] Nick Pears[1] William Smith[1] and Christian Duncan[2]
[1] Department of Computer Science, University of York, UK
[2] Alder Hey Hospital, Liverpool, UK

***Abstract*— We propose a shape template morphing approach suitable for any class of shapes that exhibits approximate reflective symmetry over some plane. The human face and full head are examples. A shape morphing algorithm that constrains all morphs to be symmetric is a form of deformation regulation. This mitigates undesirable effects seen in standard morphing algorithms that are not symmetry-aware, such as tangential sliding. Our method builds on the Coherent Point Drift (CPD) algorithm and is called Symmetry-aware CPD (SA-CPD). Global symmetric deformations are obtained by removal of asymmetric shear from CPD's global affine transformations. Symmetrised local deformations are then used to improve the symmetric template fit. These symmetric deformations are followed by Laplace-Beltrami regularized projection which allows the shape template to fit to any asymmetries in the raw shape data. The pipeline facilitates construction of statistical models that are readily factored into symmetrical and asymmetrical components. Evaluations demonstrate that SA-CPD mitigates tangential sliding problem in CPD and outperforms other competing shape morphing methods, in some cases substantially. 3D morphable models are constructed from over 1200 full head scans, and we evaluate the constructed models in terms of age and gender classification. The best performance, in the context of SVM classification, is achieved using the proposed SA-CPD deformation algorithm.**

I. INTRODUCTION

Point set registration is a key component in many tasks, such as 2D/3D image registration, morphable model construction and shape recognition. The goal is to register a *source* point set to a *target* point set, where typically the source point set is iteratively transformed and the target point set is fixed. The aim is to align the source to the target with minimal error, often requiring non-rigid deformation of the source. If the algorithm converges successfully, this yields a set of point pairs that are in close proximity across the source and target. The two shapes then have their points (or a subset of their points) in correspondence, although there will be some form of positional error distribution.

Point set registration can be used to register data to data, or some form of shape template to data - here we are interested in the latter. Thus we refer to the source point set as the *template* and the target point set as the *data*. In particular, we wish to register a 3D shape template of the human head to a collection of raw 3D images of the human head. These have missing parts and some level of noise. The end result is a set of deformed templates (one per 3D image) that share the same number of vertices and the same triangulation, as defined by the template topology. The set of deformed templates allows us to generate a statistical shape model comprised of a mean shape and the (major) modes of shape variation via the use of standard alignment techniques, such as Generalised Procrustes Analysis (GPA) and standard linear morphable model construction techniques (PCA).

The authors thank Google, in particular the project sponsor Forrester Cole, for supporting this work via Google Faculty Awards.

978-1-5386-2335-0/18/$31.00 ©2018 IEEE

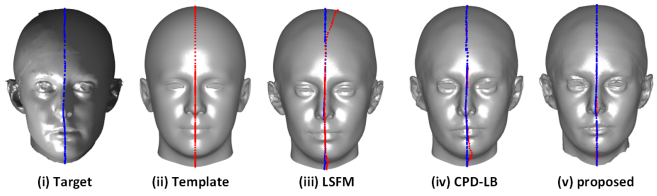

Fig. 1. Symmetry contour comparisons after template deformation. Blue points are the symmetry contour on the target data. Red points are from the symmetry contour indices of the source template. The deformed templates in (iii)-(v) show varying amounts of tangential sliding.

Our work builds on Myronenko and Song [1], who derived the Coherent Point Drift (CPD) point registration algorithm in the context of both global affine deformations (CPD-affine) and local non-rigid deformations (CPD-nonrigid). Our hypothesis is that a restriction to symmetric deformations may improve template morphing processes for (near) symmetric shapes; for example, it will not be possible for the sagittal symmetry contour of the template to deform via shearing and tangential surface sliding, which can occur in CPD-affine and CPD-nonrigid respectively.

Our approach requires strong but not perfect symmetry, as a final stage in our algorithm morphs the symmetrically deformed template to any asymmetries in the data. Therefore, our algorithm also permits the decomposition of shape into symmetric and asymmetric components, which is an interesting aspect of the study of shape variations and covariations within datasets. We call our method *Symmetry-aware CPD* (SA-CPD). Evaluations demonstrate that the proposed method outperforms other template morphing (point registration) methods in the elimination of shape difference and sliding error. As can be seen in Fig.1, the shape difference in (iii)-(v) is small. However, (iii) has a large tangential sliding error, whereas (iv) and (v) have small sliding error, with (v) being the best. The proposed method can also deal with noise, outliers, and missing data. We also provide a means to perform gender and age classification from 3D shape. The proposed template deformation method gives the best performance in both gender and age classification tasks, as compared to other leading template deformation algorithms.

In the next section we overview related work. Section

III presents our proposed SA-CPD algorithm, while Sec. IV presents our evaluations.

II. Related work

Symmetry has been studied widely in both the Computer Graphics community [2], [3] and the Computer Vision community [4], [5], [6]; for example Mitra et al's method of symmetrisation [2] is widely used and can be employed for registration of articulated bodies. However, the authors themselves state that is not suitable for computing correspondence for general models, e.g. in order to perform complex morphing operations.

The Iterative Closest Points (ICP) algorithm [7], [8] is the standard rigid-motion registration method. Several extensions of ICP for the nonrigid case were proposed [9], [10], [11], [12], [13], [14]. One such method is based on modelling the transformation with thin plate splines (TPS) [15] followed by robust point matching (RPM) and is known as TPS-RPM [16]. Amberg et al. [9] defined the optimal-step *Nonrigid Iterative Closest Points* (NICP) framework. Recently Booth et al. [10] used the same NICP template morphing approach with error pruning to built a Large Scale Facial Model (LSFM). Li et al. [17] show that using proximity heuristics to determine correspondences is less reliable when large deformations are present. Global correspondence optimization solves simultaneously for both the deformation parameters and correspondences [17].

Myronenko et al. consider the alignment of two point sets as a probability density estimation [1] and they call the method Coherent Point Drift (CPD). There is no closed-form solution for this optimisation, so it employs an EM algorithm to optimize the Gaussian Mixture Model (GMM) fitting. Algorithms are provided to solve for several shape deformation models such a affine (CPD-affine) and generally non-rigid (CPD-nonrigid). The *'non-rigid'* motion model in [1] employs an $M \times M$ Gaussian kernel $\mathbf{G}$ for motion field smoothing, and the M-step requires solving for an $M \times 3$ matrix $\mathbf{W}$ that generates the template deformation (GMM motion field) as $\mathbf{GW}$. Such motion regularisation is related to motion coherence, and inspired the algorithm's name.

The non-rigid extensions of ICP have good performance in shape difference elimination but have problems in over fitting and point sliding. TPS-RPM is slow in large-scale point set registration [18], [19], [20], [21], [22]. The CPD method was has been extended by various groups [23], [24], [25], [26]. Compared to TPS-RPM, CPD offers superior accuracy and stability with respect to non-rigid deformations in presence of outliers. A modified version of CPD imposed a *Local Linear Embedding* topological constraint to cope with highly articulated non-rigid deformations [27]. However, this extension is more sensitive to noise than CPD. A non-rigid registration method used Students Mixture Model (SMM) to do probability density estimation [28]. The results are shown to be more robust and accurate on noisy data than CPD. Dai et al. [29] proposed a hierarchical parts-based CPD-LB morphing framework to avoid under-fitting and over-fitting.

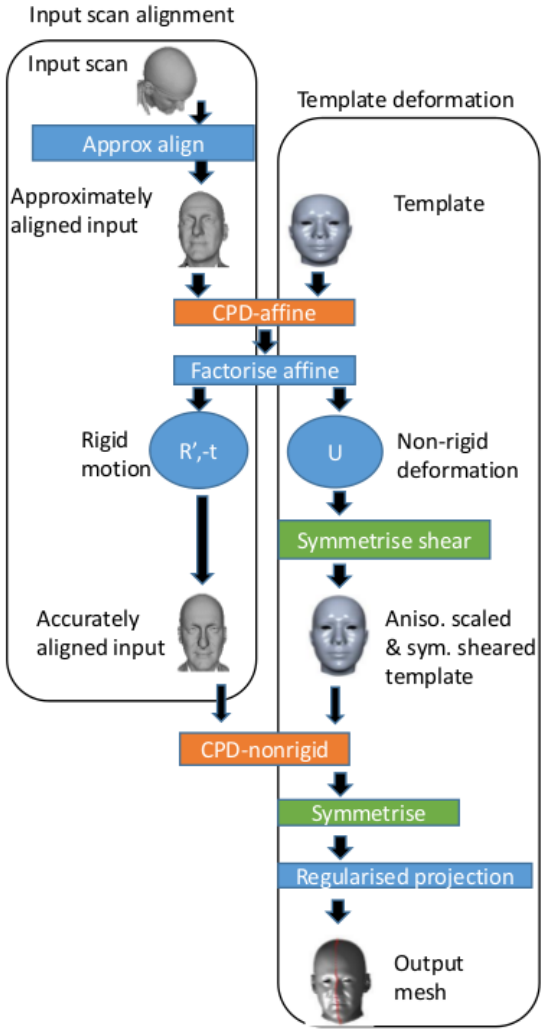

Fig. 2. Symmetry aware CPD process. The left dashed outline shows alignment processes applied to the input data. The right dashed outline shows deformation processes applied to the template data. All but the final regularised projection are symmetric deformations.

It overcomes the sliding problem to some extent, but the end result still has a small tangential sliding error.

III. Symmetry-aware Coherent Point Drift

We propose a CPD-based morphing process that only permits symmetric deformation, called *Symmetry-aware CPD* (SA-CPD). An overview of the process is shown in Fig. 2. This consists of (i) a global symmetric deformation, which is a symmetrised affine transformation, derived from CPD-affine and (ii) a local symmetric deformation, derived from CPD-nonrigid. Note that small residual asymmetries can be accounted for by using a final regularised closest-point projection of the symmetrically deformed template onto the data mesh, which is the final step shown in Fig. 2. The remainder of this section describes the component processes in Fig. 2 in more detail.

A. Approximate input scan alignment

The data in our Headspace dataset is not pose normalised and needs to be aligned to an approximate frontal pose, such that it approximately matches the pose of the template. This does not need to be accurate. It is sufficient that the initial alignment process reorientates the input scan such that it is within the convergence basin of CPD-affine. This alignment approach was described in our previous work [29]. In brief summary, our 3D input scans have an associated and registered colour-texture channel from which we detect 2D features using the approach of Zhu and Ramanan [30]. These 2D points are then projected to 3D points allowing pose normalisation by reorientating the detected 3D features to a template set of desired positions. The procedure was successful on all 1212 scans tested in the Headspace dataset.

B. CPD-affine for global symmetric deformation

The global scale parameter in CPD's so-called 'rigid' deformation formulation (a similarity transform) is often insufficiently general to give good deformation results. We prefer to use anisotropic scaling, which allows each dimension of the template to be scaled independently. Of course, the affine motion model can express this, but it also allows for XY and XZ shear, which are not permitted when the symmetry plane is at $x = 0$, although YZ shear is. The isotropically-scaled similarity motion model (termed 'rigid' in [1]) is given as:

$$T(\mathbf{y_m}; \mathbf{R}, \mathbf{t}, s) = s\mathbf{R}\mathbf{y_m} + \mathbf{t} \tag{1}$$

and the analysis to extract the optimal motion employs the orthogonality constraint $\mathbf{R^T R} = \mathbf{I}$. If we augment the isotropic scale, s, to anisotropic scaling matrix $\mathbf{S_a} = \mathbf{D}(s_x, s_y, s_z)$, and we include a symmetric shear, we have a non-rigid symmetric transformation:

$$\mathbf{U}_{sx} = \begin{bmatrix} s_x & 0 & 0 \\ 0 & s_y & m \\ 0 & 0 & s_z \end{bmatrix}, \tag{2}$$

then the motion model is more flexible than the similarity case, but is restricted to symmetric deformation and becomes:

$$T(\mathbf{y_m}; \mathbf{R}, \mathbf{U_{sx}}, \mathbf{t}) = \mathbf{R}\mathbf{U_{sx}}\mathbf{y_m} + \mathbf{t} \tag{3}$$

where the subscript sx denotes that the deformation is symmetric about the $X = 0$ plane. We can optimise for CPD's global symmetric motion $(\mathbf{R}, \mathbf{U_{sx}}, \mathbf{t})$ and variance (σ^2) parameters directly, but this is complicated as, in addition to the orthogonality constraint on $\mathbf{R}$, we need to handle the structural constraint on $\mathbf{U}_{sx}$. An alternative is to optimise with respect to a *general* affine motion, with the translation component expressed seperately, i.e. $\mathbf{T_a} = [\mathbf{B}, \mathbf{t}]$. This is a more straightforward unconstrained optimisation, and the solution is presented in [1], which here we term CPD-affine. We then determine how to extract the nearest symmetric deformation to the general affine transformation. We achieve this by decomposing the affine transformation into a rigid part (a rotation) and a non-rigid part:

$$\mathbf{B} = \mathbf{R}\mathbf{U} \tag{4}$$

where $\mathbf{U}$ is an upper-triangular matrix with anisotropic scalings on its diagonal and shears on its off-diagonal. Due to the orthogonality of $\mathbf{R}$, we have equivalent symmetric matrices such that

$$\mathbf{B}^T\mathbf{B} = \mathbf{U}^T\mathbf{U} \tag{5}$$

The known left side of the above equation is real and square-symmetric, and so we can form its Cholesky decomposition as:

$$\mathbf{B}^T\mathbf{B} = \mathbf{L}^T\mathbf{L} \tag{6}$$

and we set $\mathbf{U} = \mathbf{L^T}$ as the upper-triangular matrix representing non-rigid deformation. We then extract the rotation matrix as

$$\mathbf{R} = \mathbf{B}\mathbf{U}^{-1} \tag{7}$$

Given we have $\mathbf{U}$, we can zero any non-symmetric shears in the X-Y and X-Z planes by zeroing the off-diagonal elements, in the first row of that matrix to give a deformation matrix $\mathbf{U_{sx}}$. Finally we can reconstruct the symmetrised affine matrix from its rigid and non-rigid parts as:

$$\mathbf{B} = \mathbf{R}\mathbf{U_{sx}} \tag{8}$$

Recalling the template deformation model from Eqn. 3, we split the update across the template and data such that the (inverse) rigid part of the affine update is applied to the data and the non-rigid part is applied to the template. The intent is to maintain the template in a frame where its sagittal symmetry plane is coincident with the $X = 0$ plane, thus maintaining simplicity of form in any reflection matrix required for subsequent processing. Thus we update M template points y_m non-rigidly as:

$$\mathbf{y}_m \leftarrow \mathbf{U}_{sx}\mathbf{y}_m, \quad m = (1 \ldots M) \tag{9}$$

and N data points x_n rigidly as:

$$\mathbf{x}_n \leftarrow \mathbf{R}^T(\mathbf{x}_n - \mathbf{t}), \quad n = (1 \ldots N). \tag{10}$$

These operations are indicated in the process flow in Fig. 2.

C. CPD-nonrigid for local symmetric deformation

We now propose to find the nearest (LS sense) local symmetric deformation to the non-rigid component of any CPD-nonrigid deformation. For the required local shape deformation, we need to ensure that the displacement of proper symmetric point pairs is reflected across the symmetry plane. We assume the template maintains the pose of its symmetry plane on the YZ axis, with the inverse rigid motion being applied to the data, as described in the previous section.

Non-rigid CPD displaces the template,$\mathbf{Y}$, according to some displacement function, v:

$$\mathcal{T}(\mathbf{Y}, v) = \mathbf{Y} + v(\mathbf{Y}) \tag{11}$$

The general non-rigid motion can be considered to incorporate some (possibly zero) global-symmetric deformation.

Hence, we decompose the displacement function as global and local symmetric displacements:

$$v(\mathbf{Y}) \approx v_{sg}(\mathbf{Y}) + v_{sl}(\mathbf{Y}) \tag{12}$$

Our aim is to employ non-rigid CPD to generate the small displacements $v(\mathbf{Y})$, which can then be decomposed, to some approximation, into its symmetric global (sg) and symmetric local (sl) components. The vector field $v(\mathbf{Y})$ will be a smooth motion field, with CPD-nonrigid using a Gaussian kernel to ensure smoothness. Any (small) global symmetric deformation, $v_{sg}(\mathbf{Y})$, contained within this can be determined from the process described in Sec. III-B, using the template points before and after the non-rigid deformation as the initial points and target points of this incremental global-symmetric deformation respectively. Finally, we need to find an optimal, symmetrised, residual motion field $v_{sl}(\mathbf{Y})$ in Eqn. 12, after $v_{sg}(\mathbf{Y})$ is subtracted from $v(\mathbf{Y})$.

1) Notation: Here we define notation and suggest a simple left-right data structuring that allows a simple formulation of symmetry maintenance. We represent the template motion field as a matrix $\mathbf{V} \in \mathbb{R}^{M\times 3}$. or as a vector $\mathbf{v} \in \mathbb{R}^{3M} = \text{vec}(\mathbf{V}) = [v_{x_1}, v_{y_1}, v_{z_1}, \ldots, v_{z_M}]^T$. The mth vertex motion in the template, $\mathbf{v}_m \in \mathbb{R}^3, m \in [1, M]$ is given by $\mathbf{v}_m = [v_{3m-2}, v_{3m-1}, v_{3m}]^T$. Our CPD-based template morphing algorithm aims to maintain template extrinsic symmetry and, for any vertex motion m, its symmetric partner is given by $\text{sym}(m)$. Vertices (motions) lying on the symmetry plane are self-symmetric, i.e. $m = \text{sym}(m)$.

The template is composed of $M = 2P + S$ vertices, S of which are *self-symmetric*, leaving $P = (M - S)/2$ pairs of *proper symmetric* vertices (hence the notation P, not to be confused with probability discussed earlier). Without loss of generality, we assume that the ordering of vertices is such that the proper-symmetric vertices on one side of the mesh (e.g. left) come first, followed by the self-symmetric vertices and finally the proper-symmetric vertices on the other (e.g. right) side. Let the residual local template motions, not explained by globally symmetric deformations, be defined as;

$$v(\mathbf{Y}) - v_{sg}(\mathbf{Y}) = \mathbf{v} = \begin{bmatrix} \mathbf{v}_{\text{left}} \\ \mathbf{v}_{\text{self}} \\ \mathbf{v}_{\text{right}} \end{bmatrix} \tag{13}$$

with vertex motion selection matrices:

$$\mathbf{v}_{\text{left}} = \mathbf{S}_{\text{left}}\mathbf{v}, \quad \mathbf{v}_{\text{self}} = \mathbf{S}_{\text{self}}\mathbf{v}, \quad \mathbf{v}_{\text{right}} = \mathbf{S}_{\text{right}}\mathbf{v} \tag{14}$$

where

$$\mathbf{S}_{\text{left}} = \begin{bmatrix} \mathbf{I}_{3P} & \mathbf{0}_{3P\times 3(P+S)} \end{bmatrix} \in \{0,1\}^{3P\times 3M},$$

$$\mathbf{S}_{\text{right}} = \begin{bmatrix} \mathbf{0}_{3P\times 3(P+S)} & \mathbf{I}_{3P} \end{bmatrix} \in \{0,1\}^{3P\times 3M},$$

$$\mathbf{S}_{\text{self}} = \begin{bmatrix} \mathbf{0}_{3S\times 3P} & \mathbf{I}_{3S} & \mathbf{0}_{3S\times 3P} \end{bmatrix} \in \{0,1\}^{3S\times 3M}$$

are selection matrices that select the proper symmetric vertices from the left and right halves of the template and the self symmetric vertices respectively. The vectors $\mathbf{v}_{\text{left}}$ and $\mathbf{v}_{\text{right}}$ are assumed to appear in symmetry pair order and so the symmetry operator has a very simple form:

$$\text{sym}(m) = \begin{cases} m + P + S & \text{if } 1 \le m \le P \\ m & \text{if } P+1 \le m \le P+S \\ m - P - S & \text{if } P+S+1 \le m \le M \end{cases} \tag{15}$$

2) Proper symmetric deformation: We define a reflection in the $\mathbf{x} = \mathbf{0}$ symmetry plane by the matrix $\mathbf{F}$, where

$$\mathbf{F} = \begin{bmatrix} -1 & 0 & 0 \\ 0 & 1 & 0 \\ 0 & 0 & 1 \end{bmatrix}. \tag{16}$$

and we define $\mathbf{v}^s_{left}$ as the *symmetric-left* non-rigid local motion field that we wish to recover (symmetric deformation is distinguished from non-symmetric by the superscript). The required symmetric-right motion is recovered by a reflection of this. The reflection can be applied to the P vertices on the left side of the template motion by

$$\mathbf{G}(P) = \mathbf{I}_P \otimes \mathbf{F} \tag{17}$$

so that

$$\mathbf{v}^s_{right} = \mathbf{G}(P)\mathbf{v}^s_{left} \tag{18}$$

is the reflection of $\mathbf{v}^s_{left}$ (we use $\otimes$ to denote the Kronecker product). Then we can formulate the computation of a proper symmetric motion field as:

$$\begin{bmatrix} \mathbf{I}_P \\ \mathbf{G}(P) \end{bmatrix} \mathbf{v}^s_{left} = \begin{bmatrix} \mathbf{S}_{left} \\ \mathbf{S}_{right} \end{bmatrix} \mathbf{v} \tag{19}$$

and we solve this linear LS problem for the symmetric-left motion $\mathbf{v}^s_{left}$ and we recover the right symmetric motion as from Eqn. 18.

3) Self-symmetric deformation: Finally, we require the motion of the self-symmetric points on the template symmetry plane to be restricted to that plane. The closest in-plane motion vectors to those of CPD-non-rigid are obtained by projecting to the $x = 0$ plane with matrix, $\mathbf{P}_x$

$$\mathbf{P}_x = \begin{bmatrix} 0 & 0 & 0 \\ 0 & 1 & 0 \\ 0 & 0 & 1 \end{bmatrix}. \tag{20}$$

we define

$$\mathbf{P}_x(S) = \mathbf{I}_S \otimes \mathbf{P}_x \tag{21}$$

and the optimal S self-symmetric vertices $\mathbf{v}_{sym_s}$ are computed as:

$$\mathbf{v}^s_{self} = \mathbf{P}_x(S)\mathbf{S}_{self}\mathbf{v} \tag{22}$$

D. Regularised projection using Laplace-Beltrami

After symmetric template deformation, point projection to the aligned input data can eliminate any (normal) shape error. The template shape before and after this projection represents the symmetrised and non-symmetrised versions of template deformation respectively. Point projection is fragile if the input data is incomplete or noisy and may cause large artefacts. We overcome this by treating the projection operation as a mesh editing problem with two ingredients. First, position constraints are provided by those vertices with

mutual nearest neighbours between the deformed template and raw data. Using mutual nearest neighbours reduces sensitivity to missing data. Second, regularisation constraints are provided by the Laplace-Beltrami (LB) operator which retains the local structure of the mesh. We write the LB mesh editing problem as a linear system of equations. Given the vertices of a data scan stored in the matrix $\mathbf{X} \in \mathbb{R}^{N\times 3}$ and the deformed template obtained by CPD whose vertices are stored in the matrix $\mathbf{Y} \in \mathbb{R}^{M\times 3}$, we define the selection matrices $\mathbf{S}_1 \in [0,1]^{Q\times M}$ and $\mathbf{S}_2 \in [0,1]^{Q\times N}$ as those that select the Q vertices with mutual nearest neighbours from deformed template and data respectively. This linear system can be written as:

$$\begin{pmatrix} \lambda\mathbf{L} \\ \mathbf{S}_1 \end{pmatrix} \mathbf{Y}_{\text{proj}} = \begin{pmatrix} \lambda\mathbf{L}\mathbf{Y} \\ \mathbf{S}_2\mathbf{X} \end{pmatrix} \tag{23}$$

where $\mathbf{L} \in \mathbb{R}^{M\times M}$ is the cotangent Laplacian approximation to the LB operator and $\mathbf{Y}_{\text{proj}} \in \mathbb{R}^{M\times 3}$ are the projected vertex positions that we wish to solve for. The parameter λ weights the relative influence of the position and regularisation constraints, effectively determining the 'stiffness' of the projection. As $\lambda \to 0$, the projection tends towards nearest neighbour projection. As $\lambda \to \infty$, the deformed template will only be allowed to rigidly transform.

IV. Evaluation

We evaluate several deformation methods qualitatively and quantitatively using 1212 3D images in the Headspace dataset [29], [31], [32], which will be made public. The following subsections describe (A) qualitative and quantitative tangential sliding evaluation, (B) robustness to noise, and (C) gender and age classification performance using SVMs.

A. Tangential sliding evaluation

1) Qualitative Evaluation: We compare our method with NICP [9], the LSFM pipeline [10] (an NICP extension [9]), Li's method [17], standard CPD (affine and nonrigid) [1] and CPD-LB [29]. Fig.3 illustrates deformation methods applied to the first scan in the dataset. All methods excluding the proposed and CPD-affine have observable tangential sliding problems. However, CPD-affine by itself significantly underfits to the target shape, some form of more flexible yet non-sliding deformation is required, as is provided by our method. We apply our method to over 1212 subjects. In order to demonstrate performance, we build a 3D morphable model [33], [34] based on the deformation results. (A video is included in the supplementary material.) As shown in Fig.4, the symmetry contour is stable in the middle when shape is varied from +3SDs to -3SDs over the first ten principal components. This validates that the proposed method significantly mitigates tangential sliding over the full dataset.

2) Quantitative Evaluation: Pseudo ground truth symmetry contours are shown in blue in Fig. 1 and can be compared to the template sagittal symmetry plane contour, shown in red. We compare our method with the LSFM pipeline [10] and CPD-LB [29]. Since the correspondence between the template and data target is unknown, it is not possible to compute the correspondence error directly. Instead, we employ two metrics: 1) the Nearest Point Error (NPE) to quantify the shape difference from the deformed template to the target; 2) Symmetry Contour Error (SCE) to quantify the tangential sliding error. The NPE is computed by measuring the nearest point distance from the deformed template to raw scan and averaging over all vertices. As illustrated in Fig. 5 (a), 87% of the NPE from our method is under 1mm, which compares to 30% for CPD-LB and 28% for the LSFM pipeline. We use piecewise-trimmed ICP between the raw scan and its reflection [35] to detect the local symmetry contour (blue contour in Fig. 1) in the raw scan and we use this as a pseudo ground truth. This allows us to compute the SCE metric. (This blue symmetry contour is far less subject to surface sliding problems as it employs local-piecewise registration of the data to its self-reflection [5], and it employs robust outlier rejection. This contour can track local asymmetries, such as the nose bending to the left/right.) Fig. 5 (b) shows that 99% of SCE from our method is under 2mm, which compares to 82% for CPD-LB and 0.6% for LSFM. Overall, the proposed method significantly outperforms the other two methods across both metrics.

B. Robustness

We use a 3D data mesh with outliers, missing data and Gaussian noise to test the robustness of the proposed method. When dealing with these situations, deformation algorithms need to choose the proper parameters. So in this section, it is unfair to compare other algorithms with the proposed method, without extensive parameter tuning. We add Gaussian noise data to 100 3D meshes in the dataset. The mean of the Gaussian noise is set at the mean of the target data and variance is set to be compatible with head size,by scaling a unit normal distribution by 80mm, as shown by the blue points in Fig.7 row (3). We define 'ratio of noise' as the number of Gaussian noise points as a fraction of the number of template points, M. In Fig. 6, we demonstrate the NPE of the proposed method when dealing with different percentage of Gaussian noise. Fig.7 shows the qualitative results of the proposed method when dealing with outliers, missing data and Gaussian noise (ratio 0.6) along with error metric computations. Overall, the proposed method is robust to outliers, missing data and Gaussian noise.

C. Gender and Age Classification

We use the deformation results of the proposed SA-CPD, LSFM [10], and CPD-LB [29] to build three 3D morphable models. Then all of the 1212 face meshes in the dataset are reparameterised using each of the the models. Using the demographic information (metadata) within the Headspace dataset we train a Support Vector Machine (SVM) classifier for each model, which maps the corresponding shape vectors to the gender groups and four age groups (0-11, 12-21, 22-60 and over 60). To measure the classification accuracy, we use the classifier to predict the age bracket

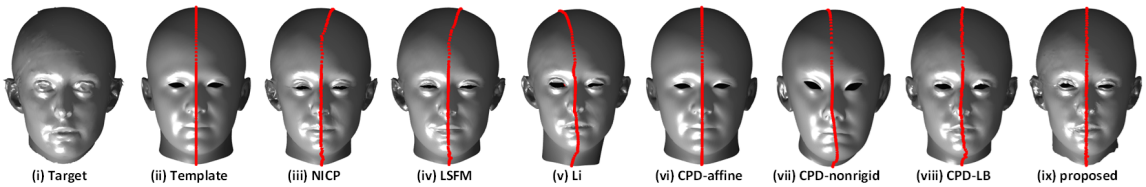

Fig. 3. Deformation of the template to the first scan using competing methods. Note the tangential sliding in all methods except the proposed and CPD-affine. CPD-affine is likely to have some small shear and significantly underfits, but the proposed method has an excellent fit to the target data.

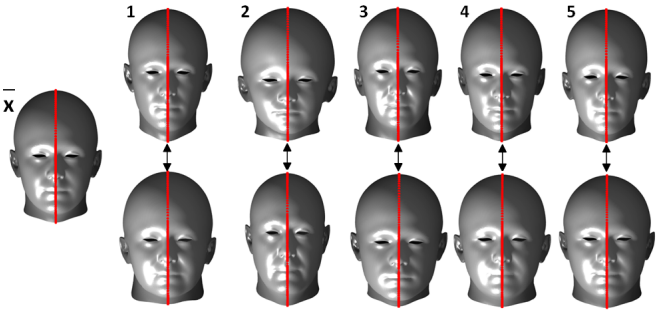

Fig. 4. 3D morphable model constructed using SA-CPD. The mean and the first five principal components are shown at +3SD (top row) and -3SD (bottom row). Note the stability of the symmetry contour, with no tangential sliding across the main eigenvectors.

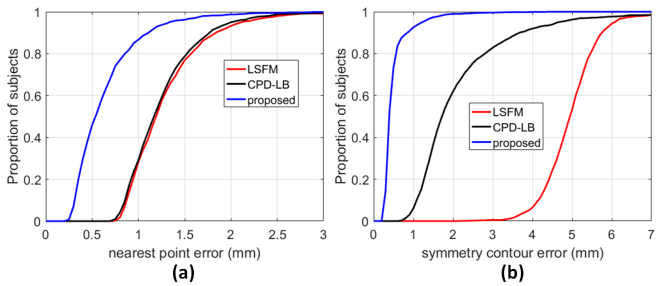

Fig. 5. (a) Proportion of subjects with a Nearest Point Error (NPE) less than abscissa value. (b) Proportion of subjects with a Symmetry Contour Error (SCE) less than abscissa value.

and the gender for the test subjects via a 10-fold cross-validation evaluation so that no test subject ever appears in the classifier's training set. This provides an application-oriented evaluation of the quality of the correspondence and low-dimensional representation. As can be seen in Table. I and II, the proposed SA-CPD deformation method has the best performance in both gender and age classification.

V. CONCLUSIONS

We proposed a Symmetry-aware Coherent Point Drift (SA-CPD) algorithm and evaluated it on 3D images of the hu-

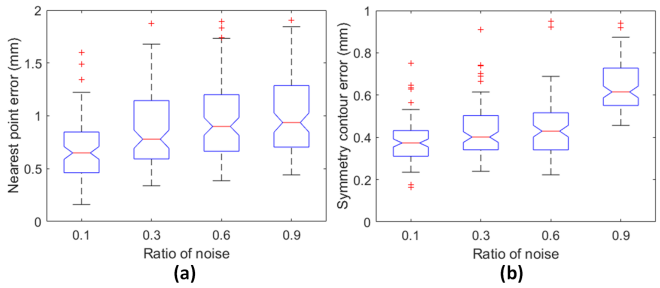

Fig. 6. (a) NPE and (b) SCE for 100 3D data scans against level of Gaussian noise.

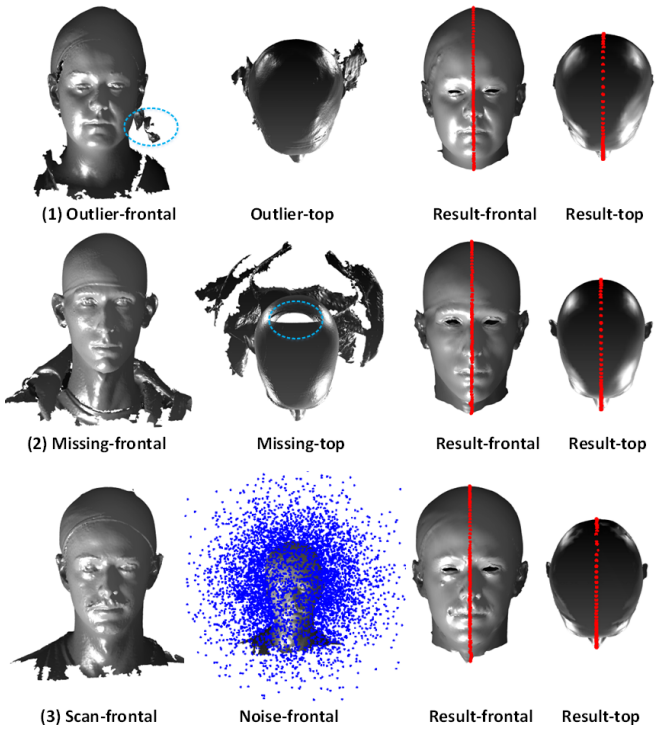

Fig. 7. Deformation results against: (1) outlier, NPE = 1.3023, SCE = 0.2843; (2) cranial data missing, NPE = 0.4418, SCE = 0.3081; (2) Gaussian noise (ratio 0.6), NPE = 0.9342, SCE = 0.6992.

TABLE I

GENDER CLASSIFICATION RESULTS

	Precision	Recall	F-score
LSFM	0.79	0.80	0.79
CPD-LB	0.81	0.81	0.81
Proposed	**0.84**	**0.84**	**0.84**

TABLE II

AGE CLASSIFICATION RESULTS

	Precision	Recall	F-score
LSFM	0.73	0.73	0.73
CPD-LB	0.73	0.74	0.73
Proposed	**0.75**	**0.76**	**0.75**

man head. This deformation method mitigates the tangential sliding problem seen in competing morphing algorithms, sometimes significantly, thereby improving the correspondence quality. The proposed method is also robust against outliers, missing data and Gaussian noise. The constructed morphable model based on the proposed deformation method has the best performance in both gender and age SVM-based classification compared to the leading competing methods. The deformation method is applicable to any shape sets that exhibit bilateral symmetry over a reflective symmetry plane.

Acknowledgements: We thank Google Faculty Awards. Headspace data collection was supported by QIDIS from the UK National Commissioning Group. We also thank Rachel Armstrong, Headspace project coordinator.

REFERENCES

[1] Myronenko, A. and Song, X., 2010. Point set registration: Coherent point drift. IEEE transactions on pattern analysis and machine intelligence, 32(12), pp.2262-2275.

[2] N. J.Mitra, L. J. Guibas, and M. Pauly., Symmetrization. ACM Trans. Graph. 26(3): 63, 2007.

[3] N. J. Mitra, M. Pauly, M. Wand, and D. Ceylan., 2012, Symmetry in Geometry: Extraction and Applications. Eurographics, 2012, pp. 29-51.

[4] Loy G., Eklundh JO. (2006) Detecting Symmetry and Symmetric Constellations of Features. In: Leonardis A., Bischof H., Pinz A. (eds) Computer Vision ECCV 2006. ECCV 2006. Lecture Notes in Computer Science, vol 3952. Springer, Berlin, Heidelberg.

[5] M. Benz, X. Laboureux, T. Maier, E. Nkenke, S. Seeger, F. W. Neukam, G. Husler., The symmetry of faces, Proceedings of the Vision, Modeling, and Visualization Conference (VMV02), Erlangen, Germany, 2002, pp. 4350.

[6] Y. Liu, K. Schmidt, J. Cohn, and S. Mitra., 2003, Facial asymmetry quantification for expression invariant human identification. Computer Vision and Image Understanding, vol 91, number 1-2, pp 138-159.

[7] Arun, K., Huang T.S., and Blostein S.D., Least squares fitting of two 3D point sets. IEEE Transactions on pattern analysis and machine intelligence vol 9, no. 5 (1987): 698-700.

[8] Besl, Paul J., and Neil D. McKay. "A method for registration of 3-D shapes." IEEE Transactions on pattern analysis and machine intelligence 14, no. 2 (1992): 239-256.

[9] Amberg, B., Romdhani, S. and Vetter, T.. Optimal step nonrigid ICP algorithms for surface registration. In Proc. CVPR, 2007, pp. 1-8.

[10] Booth, J., Roussos, A., Zafeiriou, S., Ponniah, A. and Dunaway, D., 2016. A 3d morphable model learnt from 10,000 faces. In Proceedings of the IEEE Conference on Computer Vision and Pattern Recognition (pp. 5543-5552).

[11] Hontani H, Matsuno T, Sawada Y. Robust nonrigid ICP using outlier-sparsity regularization. In Proceedings of CVPR, 2012, pp. 174-181.

[12] Cheng, S., Marras, I., Zafeiriou, S. and Pantic, M.. Active nonrigid ICP algorithm. In Automatic Face and Gesture Recognition (FG), 2015, Vol. 1, pp. 1-8.

[13] Cheng, S., Marras, I., Zafeiriou, S. and Pantic, M.. Statistical non-rigid ICP algorithm and its application to 3D face alignment. Image and Vision Computing, 2017, 58, pp.3-12.

[14] vKou, Q., Yang, Y., Du, S., Luo, S. and Cai, D.. A modified non-rigid icp algorithm for registration of chromosome images. In International Conference on Intelligent Computing, 2016 (pp. 503-513).

[15] Bookstein, Fred L. "Principal warps: Thin-plate splines and the decomposition of deformations." IEEE Transactions on pattern analysis and machine intelligence 11, no. 6 (1989): 567-585.

[16] Chui, Haili, and Anand Rangarajan. "A new algorithm for non-rigid point matching." In Computer Vision and Pattern Recognition, 2000. Proceedings. IEEE Conference on, vol. 2, pp. 44-51. IEEE, 2000.

[17] Li, H., Sumner, R.W. and Pauly, M.. Global Correspondence Optimization for NonRigid Registration of Depth Scans. In Computer graphics forum, 2008, Vol. 27, No. 5, pp. 1421-1430.

[18] Yang, J.. "The thin plate spline robust point matching (TPS-RPM) algorithm: A revisit." Patt. Rec. Letters 32, no. 7 (2011): 910-918.

[19] Lee, J.H. and Won, C.H., 2011. Topology preserving relaxation labeling for nonrigid point matching. IEEE transactions on pattern analysis and machine intelligence, 33(2), pp.427-432.

[20] Lee, A.X., Goldstein, M.A., Barratt, S.T. and Abbeel, P., 2015, May. A non-rigid point and normal registration algorithm with applications to learning from demonstrations. In Robotics and Automation (ICRA), 2015 IEEE International Conference on (pp. 935-942).

[21] Ma, J., Zhao, J., Jiang, J. and Zhou, H., 2017, February. Non-Rigid Point Set Registration with Robust Transformation Estimation under Manifold Regularization. In AAAI (pp. 4218-4224).

[22] Jiang, T., Jurie, F. and Schmid, C., Learning shape prior models for object matching. CVPR 2009. pp. 848-855

[23] Wang, P., Wang, P., Qu, Z., Gao, Y. and Shen, Z.. A refined coherent point drift (CPD) algorithm for point set registration. Science China Information Sciences, 2011, 54(12), pp.2639-2646.

[24] Golyanik, V., Taetz, B., Reis, G. and Stricker, D., 2016, March. Extended coherent point drift algorithm with correspondence priors and optimal subsampling. In Applications of Computer Vision (WACV), 2016, pp. 1-9.

[25] Hu, Y., Rijkhorst, E.J., Manber, R., Hawkes, D. and Barratt, D., September. Deformable vessel-based registration using landmark-guided coherent point drift. In International Workshop on Medical Imaging and Virtual Reality, 2010, pp. 60-69.

[26] Trimech, I.H., Maalej, A. and Amara, N.E.B., 2017, July. 3D facial expression recognition using nonrigid CPD registration method. In Information and Digital Technologies (IDT), 2017 International Conference on (pp. 478-481).

[27] Ge, S., Fan, G. and Ding, M.. Non-rigid point set registration with global-local topology preservation. In Proceedings of CVPR Workshops, 2014, pp. 245-251.

[28] Zhou, Z., Zheng, J., Dai, Y., Zhou, Z. and Chen, S.. Robust non-rigid point set registration using student's-t mixture model. PloS one, 2014, 9(3), p.e91381.

[29] H. Dai, N. Pears, W. Smith, and C. Duncan. A 3D morphable model of craniofacial shape and texture variation. In Proceedings of ICCV, 2017, pp 3085-3093.

[30] X. Zhu and D. Ramanan., Face detection, pose estimation, and landmark localization in the wild, CVPR 2012, pp. 2879–2886.

[31] Robertson, B., H. Dai, N. Pears, and C. Duncan. "A morphable model of the human head validating the outcomes of an age-dependent scaphocephaly correction." International Journal of Oral and Maxillofacial Surgery 46 (2017): 68.

[32] Alder Hey Children's Hospital Headspace Project, `http://www.alderhey.nhs.uk/departments/craniofacial/headspace-project/`.

[33] Blanz, V. and Vetter, T., 1999, July. A morphable model for the synthesis of 3D faces. In Proceedings of the 26th annual conference on Computer graphics and interactive techniques (pp. 187-194).

[34] H. Dai, W.A.P. Smith, N. Pears and C. Duncan. Symmetry-factored Statistical Modelling of Craniofacial Shape. ICCV 2017 Workshop: PeopleCap: capturing and modeling human bodies, faces and hands.

[35] Pears, N. and Duncan, C., 2016. Automatic 3D modelling of craniofacial form. arXiv preprint arXiv:1601.05593.